Original Article

Parameters of dual-energy CT for the differential diagnosis of thyroid nodules and the indirect prediction of lymph node metastasis in thyroid carcinoma: a retrospective diagnostic study

Fu Li[1#], Fuling Huang[2#], Chenmin Liu[2], Denghua Pan[3], Xiaoqi Tang[1], Yan Wen[2], Zhibai Chen[1], Yuhong Qin[2], Junqiang Chen[1,4]

[1]Department of Gastrointestinal Surgery, First Affiliated Hospital of Guangxi Medical University, Nanning, China; [2]Department of Radiology, First Affiliated Hospital of Guangxi Medical University, Nanning, China; [3]Department of Ultrasonography, First Affiliated Hospital of Guangxi Medical University, Nanning, China; [4]The Guangxi Key Laboratory of Enhanced Recovery after Surgery for Gastrointestinal Cancer, Nanning, China

Contributions: (I) Conception and design: F Li, J Chen; (II) Administrative support: F Huang, C Liu, Y Wen; (III) Provision of study materials or patients: X Tang, D Pan; (IV) Collection and assembly of data: X Tang, Z Chen; (V) Data analysis and interpretation: F Li, J Chen; (VI) Manuscript writing: All authors; (VII) Final approval of manuscript: All authors.

[#]These authors contributed equally to this work.

Correspondence to: Junqiang Chen. Department of Gastrointestinal Surgery, First Affiliated Hospital of Guangxi Medical University, 6 Shuangyong Road, Nanning 530021, China; The Guangxi Key Laboratory of Enhanced Recovery after Surgery for Gastrointestinal Cancer, Nanning, China. Email: gxmufh@163.com.

Background: To further investigate the differential diagnosis of thyroid nodules using dual-energy computed tomography (DECT) and explore the relationship between DECT parameters and lymph node metastasis in thyroid carcinoma for clinical practice, especially difficult diagnosis by routine imaging examination.

Methods: A total of 150 patients with thyroid nodules who underwent preoperative DECT and Thyroid Imaging Report and Data System (TIRADS) classification were enrolled in this study, including 96 patients with malignant tumors and 54 with benign tumors. The DECT parameters were got form regions of interest (ROI) by an experienced radiologist team and thyroid nodules and lymph node status of all patients were identified by cytology and histopathology. Statistical analyses were performed using Student's *t*-test, Chi-squared test, and receiver operating characteristic (ROC) curves.

Results: In the differential diagnosis of benign and malignant thyroid nodules, the optimal iodine concentration (IC) and normalized iodine concentration (NIC) cut-off values were IC_a (2.835 mg/mL), NIC_{1a} (0.690), and their corresponding area under the curve (AUC) were 0.940, 0.954 respectively; meantime, the optimal computed tomography (CT) value and slope of the spectral Hounsfield unit curve (λ_{HU}) cut-off values were 70 keVa (125.05 HU) and λ_{HU2a} (1.405), and their corresponding AUC were 0.955, 0.941 respectively. For lymph node status (with or without lymph node metastasis), the optimal IC and NIC thresholds were IC_a (1.715 mg/mL) and NIC_{2a} (0.155), and their corresponding AUC were 0.717, 0.720 respectively; meanwhile, the optimal CT value and λ_{HU} thresholds were 70 keVv (89.635 HU) and λ_{HU2v} (1.185), and their corresponding AUC were 0.729, 0.641 respectively.

Conclusions: Base on our study, we think DECT is useful in differentiating malignant from benign thyroid nodules, which has potential value in the indirect prediction of lymph node metastasis in thyroid carcinoma.

Keywords: Thyroid nodule; thyroid carcinoma; dual-energy computed tomography (DECT); Thyroid Imaging Report and Data System (TIRADS); lymph node metastasis

Submitted Mar 29, 2022. Accepted for publication May 18, 2022.
doi: 10.21037/gs-22-262
View this article at: https://dx.doi.org/10.21037/gs-22-262

Introduction

Thyroid nodules are common, but palpable thyroid nodules are prevalent in about 5% of women and 1% of men living in iodine-sufficient areas globally (1,2). Ultrasound (US) can detect thyroid nodules in 19–68% of the general population, which is especially higher in females and the elderly (3,4). According to a cross-sectional study in 10 cities of China, the incidence rate of thyroid nodules has increased from 2.73% in 1999 to 12.8% in 2011, especially in areas with excess iodine (5). Excluding malignant thyroid nodules, which occur in approximately 7–15% of cases depending on different risk factors, is crucial (6,7). Given the increasing incidence of thyroid nodules, differentiating malignant from benign nodules has attracted greater attention among clinical thyroid disease specialists.

US is a routine evaluation method of thyroid nodules; it is non-invasive, has good repeatability and economic efficiency ratio, and is recommended by the 2015 American Thyroid Association (ATA) guidelines (8) as well as the 2016 American Association of Clinical Endocrinologists (AACE), American College of Endocrinology (ACE), and Associazione Medici Endocrinologi (AME) medical guidelines (9). The relative US parameters and risk classifications of malignancy in the above-mentioned guidelines have excellent sensitivity and specificity for the identification of thyroid nodules, and are strongly recommended to aid decision-making about whether fine needle aspiration biopsy (FNAB) and even thyroidectomy are indicated. For improved accuracy, fine needle aspiration (FNA) procedure should be performed under US guidance. FNA results can usually be illustrated by The Bethesda System for Reporting Thyroid Cytopathology (TBSRTC) (10), which includes atypia of undetermined significance/follicular lesion of undetermined significance (AUS/FLUS) and follicular neoplasm/suspicious for follicular neoplasm (FN/SFN). TBSRTC also encompasses the diagnosis of Hürthle cell neoplasm/suspicious for and suspicious for malignancy, the above classifications are difficult to identify, and require molecular testing, repeat FNA, and even diagnostic surgery to avoid overtreatment. Therefore, there is a pressing need to develop other evaluation methods for thyroid nodules.

Dual-energy computed tomography (DECT) is a special form of computed tomography (CT), which is performed at two different energy levels and enables the identification of parameters such as iodine concentration (IC), normalized iodine concentration (NIC), CT value, as well as the slope of the spectral Hounsfield unit curve (λ_{HU}) with different voltages beyond conventional CT scans (11). Moreover, DECT can conquer the deficiencies of US and FNA, including operator dependence and invasive procedure, and so on. There are numerous reports about the evaluation of thyroid lesions and cervical lymphadenopathy with DECT. However, the conclusions are not always consistent, and are even contradictory in terms of the ICs of metastatic lymph nodes (12,13). Hence, more research is needed to identify the diagnostic value of DECT for thyroid nodules. This study aimed to further identify the differential diagnosis of thyroid nodules with DECT and explore the relationship between DECT parameters and lymph node metastasis in thyroid carcinoma. We present the following article in accordance with the STARD reporting checklist (available at https://gs.amegroups.com/article/view/10.21037/gs-22-262/rc).

Methods

Study population

The study was conducted in accordance with the Declaration of Helsinki (as revised in 2013). The study was approved by the Medical Ethics Committee of First Affiliated Hospital of Guangxi Medical University [No. 2021(KY-E-034)]. Informed consent was taken from all the patients. The US, DECT, and FNAB or pathology findings of 150 patients who underwent thyroidectomy or FNAB between April 24, 2017 and January 3, 2019 were retrospectively collected. All thyroid nodules of the patients were classified according to Thyroid Imaging Report and Data System (TIRADS) with US and underwent DECT before FNAB or surgery. Thyroid nodules and lymph node status of all patients were identified by cytology and histopathology. The baseline information of the patients with benign and malignant thyroid nodules in this study is displayed in *Table 1*.

Conventional US examination

All patients underwent routine US of the thyroid using the following equipment: LOGIQ E9 US equipment (GE, USA) with a linear probe (6–15 MHz). The patients were placed flat on their backs with full exposure of their neck. US was performed to record the nodules' data, including composition, echogenicity, shape, margin, echogenic foci of TIRADS classification (14,15), and other baseline features.

Table 1 Baseline information of patients with benign and malignant thyroid nodules

Patients	Benign nodules	Malignant nodules	P value
Number	54	103	–
Gender (female), n	47	80	0.198
Age (years), mean ± SD	44.72±12.32	40.45±12.03	0.04
Nodule size (millimeter), mean ± SD	2.46±1.26	1.55±1.24	0.00

SD, standard deviation.

Further classified criteria of Kwak *et al.* (16) were also used in this study.

TIRADS classification:

- TIRADS 1: 0 points; normal thyroid;
- TIRADS 2: 1 point; no malignant sign, benign lesions;
- TIRADS 3: 3 points; no malignant sign, high probability of benignity;
- TIRADS 4a: 4 points; one malignant sign, possible benignity;
- TIRADS 4b: 5 points; two malignant signs, possible malignancy;
- TIRADS 4c: 6 points; three or four malignant signs, high possibility of malignancy;
- TIRADS 5: ≥7 points; five malignant signs, highly indicative of malignancy.

Image analysis of US

All procedures were performed by an experienced radiologist team with over 7 years of clinical practice in US and diagnosis of thyroid nodules. Two experienced radiologists of the team completed the US imaging analysis and TIRADS classification, respectively, without knowing the pathological results. A third senior specialist reviewed the data and excluded possible disagreements.

Dual-source DECT examination

All of the included patients underwent CT scanning using a dual-source DECT model (17) (Siemens SOMATOM Definition Flash CT, Germany). The patients were placed on the scanning bed, avoided swallowing during the examination, and double energy non-enhanced phase and enhanced arterial/venous phases scans were then performed according to the following parameters: tube voltage, 100 keV; B tube voltage, Sn140 keV; tube current, 180 mAs; starting CARE Dose4D at the same time; rotation speed, 0.28 s; helical pitch, 0.55; dual energy fusion coefficient, 0.4; reconstruction layer thickness, 1.5 mm; and layer spacing, 1.5 mm. The scan ranged from the cranial top to the thoracic entrance. For contrast material-enhanced scanning, an iodinated nonionic contrast agent (iopamidol 300; Bracco, Milan, Italy) was injected through the right elbow median vein at 3 mL/s by using a double-tube and high-pressure injector (85 mL; Nemoto Kyorindo Co., Ltd., Tokyo, Japan). The scan delay times for the arterial and venous phases were 25 and 60 s, respectively.

DECT image analysis

The images were transmitted to MMWP workstation, and the "Liver-VNC" mode was selected to obtain iodine-based material decomposition maps. The regions of interest (ROI) were placed on the core area of lesion, normal thyroid gland, and the common carotid artery on the cross-sectional maps, avoiding obvious calcification, cyst, necrosis, large blood vessels, and lesion margins. All mean values of the lesion and normal thyroid gland were obtained from three typical, consecutive layers, and those of the common carotid artery were obtained from a two-thirds range of the core area. All images were analyzed by an experienced radiologist team, with over 10 years of experience in CT diagnostics. A third senior radiologist was invited to deal with possible disagreement. The DECT parameters were abbreviated as follows: p = plain scan phase, a = arterial scan phase, v = venous scan phase. Plain scan phase: $IC_p = IC_{lesion}$, $IC_n = IC_{normal\ thyroid\ tissue}$, $IC_c = IC_{common\ carotid\ artery}$, $NIC_{1p} = NIC_{lesion/normal\ thyroid\ tissue}$, $NIC_{2p} = NIC_{lesion/common\ carotid\ artery}$, $\lambda_{HU1p} = (HU_{40keV} - HU_{100keV})/(100 - 40)$, $\lambda_{HU2p} = (HU_{70keV} - HU_{100keV})/(100 - 70)$; arterial scan phase: $IC_a = IC_{lesion}$, $IC_n = IC_{normal\ thyroid\ tissue}$, $IC_c = IC_{common\ carotid\ artery}$, $NIC_{1a} = NIC_{lesion/normal\ thyroid\ tissue}$, $NIC_{2a} = NIC_{lesion/common\ carotid\ artery}$, $\lambda_{HU1a} = (HU_{40keV} - HU_{100keV})/(100 - 40)$, $\lambda_{HU2a} = (HU_{70keV} - HU_{100keV})/(100 - 70)$; venous scan phase: $IC_v = IC_{lesion}$, $IC_n = IC_{normal\ thyroid\ tissue}$, $IC_c = IC_{common\ carotid\ artery}$, $NIC_{1v} = NIC_{lesion/normal\ thyroid\ tissue}$, NIC_{2v}

Table 2 Histopathological or cytopathological results of 150 patients

Pathologic types	Patients (n=150)
Benign nodules	54
Nodular goiter	38
Adenomatous nodular goiter	7
Adenoma	4
Hashimoto's thyroiditis	3
Cyst	2
Malignant nodules	96
Papillary carcinoma	93
Medullary carcinoma	2
Anaplastic carcinoma	1

$= NIC_{lesion/common\ carotid\ artery}$, $\lambda_{HU1v} = (HU_{40keV} - HU_{100keV})/(100 - 40)$; and $\lambda_{HU2v} = (HU_{70keV} - HU_{100keV})/(100 - 70)$.

FNAB cytology and histopathology

Patients evaluated to be ≥ TIRADS 4a underwent US-guided FNAB preoperatively using a 23-G gauge needle by the same radiologist team. After continuous suction for 4–5 times in the core of the lesion with negative pressure, the specimen was put on clean slide, immediately smeared, and fixed with 95% alcohol. Biopsy was repeated 3–4 times for each lesion. All specimens were dyed and diagnosed as benign, malignant, or intermediate outcomes by the experienced pathologists. In this study, only definite benign and malignant cytopathological results were adopted the as final diagnostic standard because of patient's rejecting operation.

Statistical analysis

The SPSS 22.0 statistical package (Chicago, IL, USA) was used to perform statistical analysis. Qualitative data was analyzed with Chi-squared test. The independent-samples *t*-test was used to compare the DECT parameters as well as the TIRADS scores between benign and malignant thyroid nodules, and analyze the DECT parameters in thyroid carcinomas with and without lymph node metastasis. A receiver operating characteristic (ROC) curve was used to differentiate benign from malignant thyroid nodules and predict lymph node metastasis of thyroid carcinoma. P<0.05 was considered as significantly different for all statistical analyses in this study.

Results

A total of 150 patients were enrolled were enrolled in this study, including 54 with benign lesions and 96 with malignant lesions. The pathological outcomes are shown in *Table 2*.

The IC of lesions in malignant nodules were lower than those in benign nodules at the plain, arterial, and venous scan phases (P<0.05), especially in arterial scan phase. Also, NIC_1 and NIC_2 showed the same pattern, which were significantly different (P<0.05). The IC, NIC_1, and NIC_2 of normal thyroid glands with benign and malignant thyroid nodules were not obviously different in the three above phases (P>0.05). Furthermore, the IC, NIC_1, and NIC_2 of common carotid arteries with benign and malignant thyroid nodules were not significantly different in the same scan phases (P>0.05). The specific results are shown in *Table 3*.

Different CT values, λ_{HU1}, and λ_{HU2} of lesions with 40, 70, 100 keV in malignant nodules were significantly lower than those in benign nodules at the plain, arterial, and venous scan phases respectively (P<0.05), the corresponding outcomes are displayed in *Table 4*. However, different CT values, λ_{HU1}, and λ_{HU2} of normal thyroid gland with 40, 70, 100 keV were without the same pattern; only λ_{HU2p}, CT_{40keVa}, CT_{70keVa}, λ_{HU1a}, λ_{HU2a}, and CT_{40keVv} showed a significant difference between benign and malignant thyroid nodules (P<0.05), and the related data is displayed in *Table 5*. This may be due to the influence of a portion of patients with background of nodular goiter on the measuring results of relatively normal thyroid gland tissue.

All of the patients were classified with TIRADS, but malignancy was only in TIRADS 3 to 5, and the corresponding malignancy rates were 13.95%, 50.00%, 80.77%, 97.30%, and 96.00%, respectively. The distribution of thyroid nodules with different TIRADS is shown in *Table 6*.

Table 7 displays the ROC curves analysis of different IC, NIC, and TIRADS classification for the differential diagnosis of thyroid nodules. In our study, the area under the curves (AUCs) of IC_a, NIC_{1a}, and NIC_{2a} were 0.940, 0.954, and 0.949, respectively, in the arterial phase; the AUCs of IC_v, NIC_{1v}, NIC_{2v} were 0.925, 0.912, and 0.915, respectively, in the venous phase; and the AUC of TIRADS was 0.910, without the advantage of comparing with the aforementioned index, but obviously superior to the AUCs of IC_p, NIC_{1p}, and NIC_{2p} in the plain phase. *Figures 1,2*

Table 3 Comparison of IC and NIC in benign and malignant thyroid nodules

Iodine concentration (mg/mL)	Benign nodules, mean ± SD	Malignant nodules, mean ± SD	P value
Plain scan phase			
IC_p	1.15±0.88	0.17±0.90	0.000
IC_n	1.74±0.94	1.79±1.05	0.783
IC_c	0.61±1.17	0.73±1.22	0.556
NIC_{1p}	0.78±0.64	0.05±0.76	0.000
NIC_{2p}	1.63±4.47	−1.19±5.32	0.001
Arterial scan phase			
IC_a	4.84±1.78	1.63±1.38	0.000
IC_n	5.18±1.22	5.45±1.11	0.170
IC_c	10.75±2.07	10.76±2.24	0.973
NIC_{1a}	0.97±0.40	0.30±0.25	0.000
NIC_{2a}	0.45±0.16	0.15±0.13	0.000
Venous scan phase			
IC_v	4.19±1.54	1.60±1.18	0.000
IC_n	4.60±1.09	4.50±1.00	0.590
IC_c	5.03±1.42	5.14±1.47	0.656
NIC_{1v}	0.91±0.39	0.36±0.28	0.000
NIC_{2v}	0.80±0.43	0.36±0.54	0.000

IC, iodine concentration; NIC, normalized iodine concentration; SD, standard deviation.

showed the same results.

Table 8 shows the ROC curves analysis of different CT values, λ_{HU} with different voltages, and TIRADS classification for the differential diagnosis of thyroid nodules. AUC of CT_{40keVa}, CT_{70keVa}, $CT_{100keVa}$, λ_{HU1a}, and λ_{HU2a} were 0.950, 0.955, 0.926, 0.941, and 0.942, respectively, in the arterial phase, which was superior to the AUC with TIRADS (0.910). The AUCs of CT_{40keVv}, CT_{70keVv}, and $CT_{100keVv}$ were 0.927, 0.948, and 0.921, respectively, which signified an advantage over US. The other indicators in the different phases were inferior to US. The corresponding outcomes are shown in *Figures 1*,*3*.

The IC_a, NIC_{1a}, and NIC_{2a} of lesions in thyroid carcinomas with lymph node metastasis (LN+) group were lower than those without lymph node metastasis (LN−) at the arterial scan (P<0.05). The IC_v and NIC_{1v} revealed the same result at the venous scan phases (P<0.05). The other indicators were not obviously different in the three phases mentioned above (P>0.05). The related results were showed in *Table 9*.

The CT values of thyroid carcinoma lesions with 40, 70, and 100 keV in the LN+ group were markedly lower than those in the LN− group at the arterial and venous scan phases, respectively (P<0.05). Only λ_{HU1v} and λ_{HU2v} revealed the same change at the venous scan phase; the other indicators were not obviously different in the three phases (P>0.05). The corresponding outcomes are shown in *Table 10*.

Table 11 displays the ROC curves analysis of different DECT parameters in thyroid carcinomas with and without lymph node metastasis. In this study, the AUC of IC_a, NIC_{1a}, NIC_{2a}, IC_v, NIC_{1v}, CT_{40keVa}, CT_{70keVa}, $CT_{100keVa}$, CT_{40keVv}, CT_{70keVv}, $CT_{100keVv}$, λ_{HU1v}, and λ_{HU2v} were 0.717, 0.709, 0.720, 0.648, 0.616, 0.668, 0.703, 0.709, 0.661, 0.729, 0.711, 0.631, and 0.641, respectively with different sensitivities and specificities at the arterial and venous scan phases. The same results are shown in *Figure 4*.

Discussion

According to data from the Global Cancer Statistics 2018 (18),

Table 4 Comparison of the CT value and λ_{HU} with different voltages in benign and malignant thyroid nodules for lesion tissues

CT value (HU) and λ_{HU}	Benign nodules, mean ± SD	Malignant nodules, mean ± SD	P value
Plain scan phase			
CT_{40keVp}	144.63±63.53	63.58±67.81	0.000
CT_{70keVp}	81.51±18.91	48.20±20.12	0.000
$CT_{100keVp}$	65.26±12.03	44.34±14.69	0.000
λ_{HU1p}	1.32±1.00	0.32±1.10	0.000
λ_{HU2p}	0.54±0.41	0.13±0.45	0.000
Arterial scan phase			
CT_{40keVa}	447.47±141.49	184.04±112.24	0.000
CT_{70keVa}	174.33±42.20	88.24±37.68	0.000
$CT_{100keVa}$	103.94±18.41	63.47±22.95	0.000
λ_{HU1a}	5.73±2.10	2.01±1.04	0.000
λ_{HU2a}	2.35±0.86	0.83±0.67	0.000
Venous scan phase			
CT_{40keVv}	395.43±120.27	176.96±105.94	0.000
CT_{70keVv}	156.87±33.13	85.89±34.25	0.000
$CT_{100keVv}$	96.29±15.01	62.30±23.22	0.000
λ_{HU1v}	4.99±1.83	1.91±1.62	0.000
λ_{HU2v}	2.02±0.73	0.79±0.66	0.000

CT, computed tomography; λ_{HU}, slope of the spectral Hounsfield unit curve; SD, standard deviation.

there were 567,000 new cases of thyroid carcinoma in the world. Although the mortality rate of thyroid carcinoma was stable and low, recurrence and metastasis remain an unavoidable topic. The first step is to differentiate malignant from benign thyroid nodules. To our knowledge, many imaging technique modalities have been used to diagnose thyroid nodules, including US, CT, magnetic resonance imaging (MRI), single photon emission CT (SPECT), and positron emission tomography (PET)/CT. US is recommended as the best examination for screening and preoperative evaluation, while conventional US combined with contrast-enhanced US could further improve the accuracy from 90.3% to 96% in the diagnosis of thyroid nodules (19). Moreover, elastosonography based on conventional US is useful for the diagnosis of thyroid nodules (20). However, US is limited by large, multiple thyroid nodules and retrosternal goiter, and it depends on operator's experience heavily (21). Conventional CT involves mixed energy imaging for a good signal to noise ratio. Meanwhile, DECT provides more information beyond conventional CT without obviously influencing the quality of imaging, including CT values with voltage series, IC, and λ_{HU}. The more detailed information provided by DECT assists in the accurate diagnosis of thyroid nodules, as shown in the examples displayed in *Figures 5*,*6*.

Iodine uptake is characteristic of the thyroid, which is influenced by the formation of thyroid nodules. Dohán *et al.* (22) reported a decreasing iodine uptake in thyroid cancer. This finding was confirmed by series of reports (23-28), and was used to differentiate malignant from benign thyroid nodules. In the present study, the IC, NIC_1, and NIC_2 of lesions in malignant nodules were lower than those in benign nodules at the plain, arterial, and venous scan phases, especially in the arterial scan phase, which is consistent with the results of the above-mentioned studies. The optimal IC_a, NIC_{1a}, and NIC_{2a} cut-offs for the differential diagnosis of malignancy and benignity in the arterial scan phase were 2.835 mg/mL, 0.690, and 0.275, respectively, which had an advantage over TIRADS (sensitivity: 87.50%, 96.90%, 89.60% *vs.* 84.40%; specificity: 92.60%, 87.00%, 90.70% *vs.* 87.00%).

Table 5 Comparison of the CT value and λ_{HU} with different voltages in benign and malignant thyroid nodules for normal thyroid tissue

CT value (HU) and λ_{HU}	Benign nodules, mean ± SD	Malignant nodules, mean ± SD	P value
Plain scan phase			
CT_{40keVp}	202.84±64.33	221.77±74.91	0.121
CT_{70keVp}	103.10±18.92	107.29±22.66	0.251
$CT_{100keVp}$	77.22±10.84	77.63±12.83	0.845
λ_{HU1p}	2.09±1.00	2.40±1.04	0.098
λ_{HU2p}	0.86±0.41	2.59±0.43	0.000
Arterial scan phase			
CT_{40keVa}	479.52±91.52	514.90±84.69	0.018
CT_{70keVa}	190.38±28.05	199.59±26.21	0.046
$CT_{100keVa}$	115.84±13.47	117.44±13.44	0.485
λ_{HU1a}	6.06±1.35	6.63±1.25	0.011
λ_{HU2a}	2.49±0.55	2.74±0.52	0.006
Venous scan phase			
CT_{40keVv}	436.55±74.61	431.62±75.58	0.700
CT_{70keVv}	173.09±23.00	172.81±21.03	0.941
$CT_{100keVv}$	105.22±11.77	105.09±10.23	0.945
λ_{HU1v}	5.52±1.11	5.44±1.16	0.681
λ_{HU2v}	2.26±0.46	2.26±0.46	0.949

CT, computed tomography; λ_{HU}, slope of the spectral Hounsfield unit curve; SD, standard deviation.

Table 6 TIRADS classifications of benign and malignant thyroid nodules for all patients

TIRADS classifications	TIRADS score	Benign nodules	Malignant nodules	Number of cases	Malignancy rate, %
TIRADS 2	2	1	0	1	0.00
TIRADS 3	3	37	6	43	13.95
TIRADS 4a	4	9	9	18	50.00
TIRADS 4b	5	5	21	26	80.77
TIRADS 4c	6	1	36	37	97.30
TIRADS 5	7	1	24	25	96.00
Total	–	54	96	150	–

TIRADS, Thyroid Imaging Report and Data System.

Virtual monochromatic images (VMIs) were reconstructed using the workstation's corresponding software. In this study, we acquired VMI energies ranging from 40 to 190 keV with dual-source DECT. Seventy keV VMI was comprehensively accepted as a relatively standard energy level for routine reconstruction (29-31). Low energy VMI can increase visualization of tumors and their edges (32), and thus, 40 keV VMI was applied in our study to diagnose thyroid nodules. One hundred keV VMI was selected as the representative of high-energy images for analysis. Our study showed the CT value, λ_{HU1}, and λ_{HU2} of lesions with 40, 70, and 100 keV in malignant nodules were

Table 7 ROC curves analysis of different IC, NIC, and TIRADS classification for the differential diagnosis of thyroid nodules (IC mg/mL)

Diagnostic parameters	IC_p	NIC_{1p}	NIC_{2p}	IC_a	NIC_{1a}	NIC_{2a}	IC_v	NIC_{1v}	NIC_{2v}	TIRADS
AUC	0.809	0.821	0.727	0.940	0.954	0.949	0.925	0.912	0.915	0.910
Cutoff value	0.550	0.495	0.905	2.835	0.690	0.275	3.00	0.650	0.575	4.5
Sensitivity, %	70.80	86.50	86.50	87.50	96.90	89.60	89.60	90.60	88.50	84.40
Specificity, %	77.80	66.70	61.10	92.60	87.00	90.70	90.70	90.7	90.7	87.0
P value	0.000	0.000	0.000	0.000	0.000	0.000	0.000	0.000	0.000	0.000

ROC, receiver operating characteristic; IC, iodine concentration; NIC, normalized iodine concentration; TIRADS, Thyroid Imaging Report and Data System; AUC, area under the curve.

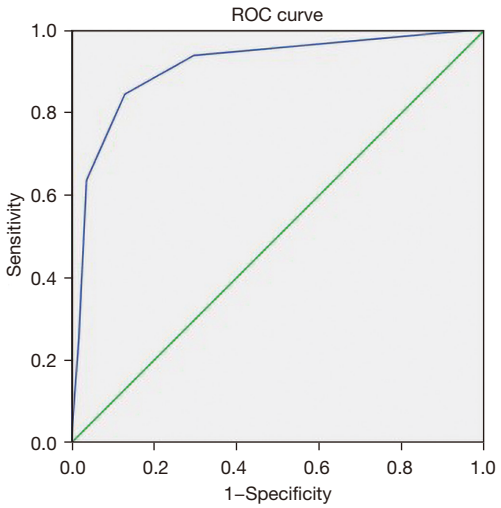

Figure 1 ROC for the differential diagnosis of benign and malignant thyroid nodules with TIRADS score in this study (cutoff: 4.5). ROC, receiver operating characteristic; TIRADS, Thyroid Imaging Report and Data System.

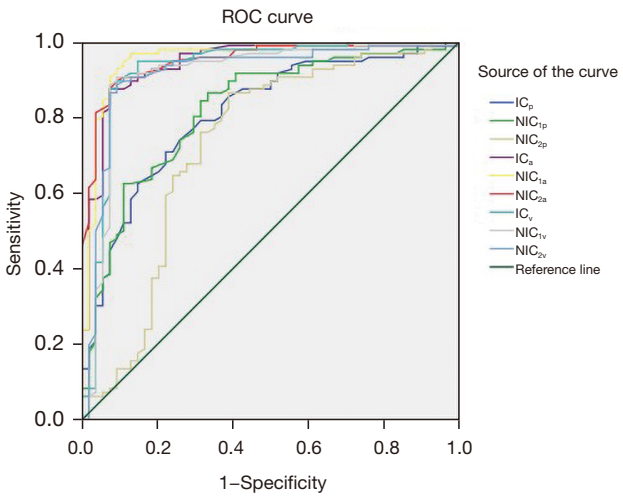

Figure 2 ROC for differential diagnosis of benign and malignant thyroid nodules with different IC and NIC in this study. ROC, receiver operating characteristic; IC, iodine concentration; NIC, normalized iodine concentration.

Table 8 ROC curves analysis of different CT value (HU), λ_{HU}, and TIRADS classification for the differential diagnosis of thyroid nodules

Diagnostic parameters	CT_{40keVp}	CT_{70keVp}	$CT_{100keVp}$	λ_{HU1p}	λ_{HU2p}	CT_{40keVa}	CT_{70keVa}	$CT_{100keVa}$	λ_{HU1a}	λ_{HU2a}	CT_{40keVv}	CT_{70keVv}	$CT_{100keVv}$	λ_{HU1v}	λ_{HU2v}	TIRADS
AUC	0.845	0.897	0.865	0.781	0.778	0.950	0.955	0.926	0.941	0.942	0.927	0.948	0.921	0.906	0.903	0.910
Cutoff value	91.25	64.60	54.90	0.755	0.245	313.515	125.05	86.515	3.41	1.405	304.115	130.665	84.75	3.58	1.465	4.5
Sensitivity, %	70.80	87.50	79.20	68.80	62.50	91.70	88.50	88.50	86.50	87.50	90.60	95.80	86.50	88.50	88.50	84.40
Specificity, %	87.00	85.20	85.20	79.60	85.20	87.00	90.70	85.20	90.70	90.70	85.20	85.20	85.20	85.20	83.30	87.0
P value	0.000	0.000	0.000	0.000	0.000	0.000	0.000	0.000	0.000	0.000	0.000	0.000	0.000	0.000	0.000	0.000

ROC, receiver operating characteristic; CT, computed tomography; λ_{HU}, slope of the spectral Hounsfield unit curve; TIRADS, Thyroid Imaging Report and Data System; AUC, area under the curve.

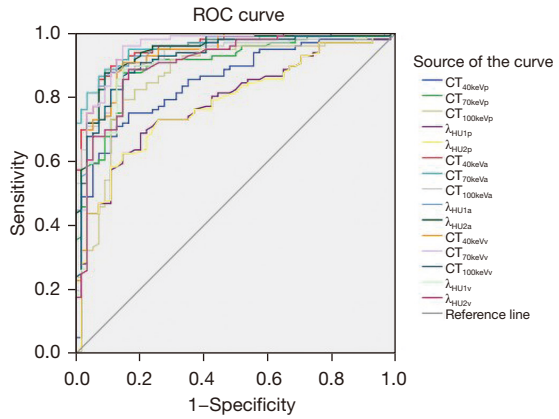

Figure 3 ROC for the differential diagnosis of benign and malignant thyroid nodules with different CT values and λ_{HU} in this study. ROC, receiver operating characteristic; CT, computed tomography; λ_{HU}, slope of the spectral Hounsfield unit curve.

significantly lower than those in benign nodules at the plain, arterial, and venous scan phases, respectively, especially in the arterial scan phase, which is consistent with previous studies (mentioned above). The optimal cut-off for the differential diagnosis of malignancy and benignity in arterial scan phase with CT_{40keVa}, CT_{70keVa}, $CT_{100keVa}$, λ_{HU1a}, and λ_{HU2a} were 313.515, 125.050, 86.515, 3.41, and 1.405, respectively, which was superior to TIRADS (sensitivity: 91.70%, 88.50%, 88.50%, 86.50%, 87.50% *vs.* 84.40%; specificity: 87.00%, 90.70%, 85.20%, 90.70%, 90.70% *vs.* 87.00%).

In clinical practice, different surgical strategies are indicated for thyroid carcinomas with or without lymph node metastasis. Metastatic lymph node lesions also exhibit the feature of iodine uptake, which was used to identify lymph node metastasis in thyroid carcinoma using DECT, especial for the differentiation of cervical lymph node

Table 9 Comparison of IC and NIC in thyroid carcinoma LN+ and LN–

IC (mg/mL)	Thyroid carcinoma LN–, mean ± SD	Thyroid carcinoma LN+, mean ± SD	P value
Plain scan phase			
IC_p	0.19±0.87	0.16±0.92	0.894
IC_n	1.79±1.09	1.78±1.03	0.983
IC_c	0.54±0.88	0.87±1.40	0.180
NIC_{1p}	0.12±0.96	–0.01±0.58	0.396
NIC_{2p}	–2.15±6.84	–0.50±3.82	0.172
Arterial scan phase			
IC_a	2.04±1.25	1.34±1.40	0.013
IC_n	5.46±1.00	5.45±1.20	0.960
IC_c	10.77±2.13	10.76±2.34	0.985
NIC_{1a}	0.37±0.24	0.25±0.25	0.018
NIC_{2a}	0.18±0.13	0.12±0.13	0.020
Venous scan phase			
IC_v	1.97±1.04	1.33±1.17	0.008
IC_n	4.66±0.78	4.39±1.12	0.184
IC_c	5.26±1.31	5.05±1.58	0.501
NIC_{1v}	0.43±0.24	0.31±0.29	0.028
NIC_{2v}	0.37±0.22	0.35±0.28	0.865

IC, iodine concentration; NIC, normalized iodine concentration; LN–, without lymph node metastasis; LN+, with lymph node metastasis; SD, standard deviation.

Table 10 Comparison of the CT value and λ_{HU} with different voltages in thyroid carcinoma LN+ and LN–

CT value (HU) and λ_{HU}	Thyroid carcinoma LN–, mean ± SD	Thyroid carcinoma LN+, mean ± SD	P value
Plain scan phase			
CT_{40keVp}	69.28±62.07	59.52±71.91	0.479
CT_{70keVp}	51.07±20.21	46.15±19.99	0.240
$CT_{100keVp}$	46.31±15.34	42.93±14.18	0.268
λ_{HU1p}	0.38±0.99	0.28±1.17	0.642
λ_{HU2p}	0.16±0.41	0.11±0.47	0.583
Arterial scan phase			
CT_{40keVa}	212.13±97.46	163.99±118.50	0.038
CT_{70keVa}	99.19±34.69	80.43±38.07	0.015
$CT_{100keVa}$	70.09±23.52	58.74±21.50	0.016
λ_{HU1a}	2.37±1.42	1.75±1.75	0.071
λ_{HU2a}	0.97±0.58	0.72±0.72	0.77
Venous scan phase			
CT_{40keVv}	211.12±101.61	152.56±103.00	0.007
CT_{70keVv}	99.97±32.50	75.83±32.09	0.000
$CT_{100keVv}$	70.90±22.17	56.15±22.14	0.002
λ_{HU1v}	2.34±1.56	1.61±1.62	0.029
λ_{HU2v}	0.97±0.63	0.66±0.66	0.022

CT, computed tomography; λ_{HU}, slope of the spectral Hounsfield unit curve; LN–, without lymph node metastasis; LN+, with lymph node metastasis; SD, standard deviation.

Table 11 ROC analysis of the different parameters of DECT in thyroid carcinomas with and without lymph node metastasis (IC mg/mL, CT value HU)

Diagnostic parameters	IC_a	NIC_{1a}	NIC_{2a}	IC_v	NIC_{1v}	CT_{40keVa}	CT_{70keVa}	$CT_{100keVa}$	CT_{40keVv}	CT_{70keVv}	$CT_{100keVv}$	λ_{HU1v}	λ_{HU2v}
AUC	0.717	0.709	0.720	0.648	0.616	0.668	0.703	0.709	0.661	0.729	0.711	0.631	0.641
Cutoff value	1.715	0.385	0.155	1.40	0.145	198.00	72.535	60.35	193.265	89.635	60.45	2.995	1.185
Sensitivity, %	71.40	85.70	73.20	48.20	28.60	73.20	46.40	58.90	64.30	69.60	53.60	80.40	78.60
Specificity, %	70.00	45.00	65.00	75.00	95.00	62.50	90.00	80.00	62.50	72.50	85.00	42.50	45.00
P value	0.000	0.000	0.000	0.014	0.053	0.005	0.001	0.000	0.007	0.000	0.000	0.029	0.019

ROC, receiver operating characteristic; DECT, dual-energy computed tomography; IC, iodine concentration; CT, computed tomography; NIC, normalized iodine concentration; λ_{HU}, slope of the spectral Hounsfield unit curve; AUC, area under the curve.

metastasis (33). Despite previous reports about higher IC, NIC, and λ_{HU} in metastatic lymph nodes compared to non-metastatic lymph nodes in thyroid carcinoma (34-36), it was difficult to measure the parameters of all lymph nodes for all patients, and a portion of the lymph nodes were illegible. It was relatively easy and feasible to measure the lesion of thyroid carcinoma, which may indirectly reflect the status of the lymph nodes in thyroid carcinoma. In this study, the IC_a, NIC_{1a}, and NIC_{2a} of lesions in thyroid carcinomas in the LN+ group were significantly lower than those in the LN– group at the arterial scan phase. Meanwhile, IC_v and NIC_{1V} exhibited the same result at the

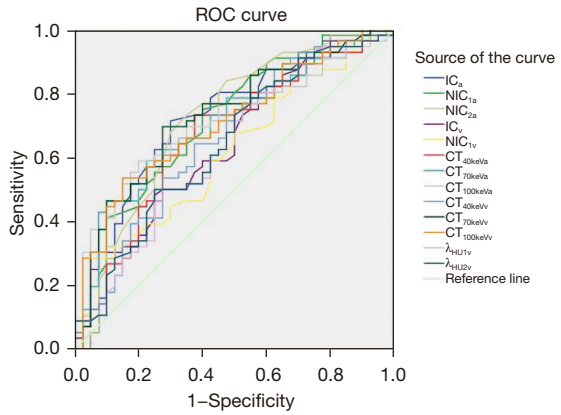

Figure 4 ROC analysis of the different DECT parameters in thyroid carcinomas with and without lymph node metastasis. ROC, receiver operating characteristic; IC, iodine concentration; NIC, normalized iodine concentration; CT, computed tomography; λ_{HU}, slope of the spectral Hounsfield unit curve; DECT, dual-energy computed tomography.

venous scan phase. There was no difference in NIC_{V2} for both groups. The CT values of thyroid carcinoma lesions with 40, 70, and 100 keV in the LN+ group were obviously lower than those in the LN− group at the arterial and venous scan phases, respectively; however, λ_{HU1v} and λ_{HU2v} showed the same change only at the venous scan phase. The optimal parameter for the differential status of lymph nodes in thyroid carcinomas with iodine was NIC_{2a} (0.155, sensitivity: 73.20%, specificity: 65.00%). The optimal threshold for the differential status of lymph nodes in thyroid carcinomas with VMI was 89.635 (70 keV at venous phase, sensitivity: 69.60%, specificity: 72.50%). The latter was the optimal parameter for the differential status of lymph nodes in thyroid carcinomas by ROC analysis, which was affirmed by a previous report (37), which found that the venous phase contributed to the identification of lymph node metastasis in thyroid carcinoma.

At present, not much more is known about DECT.

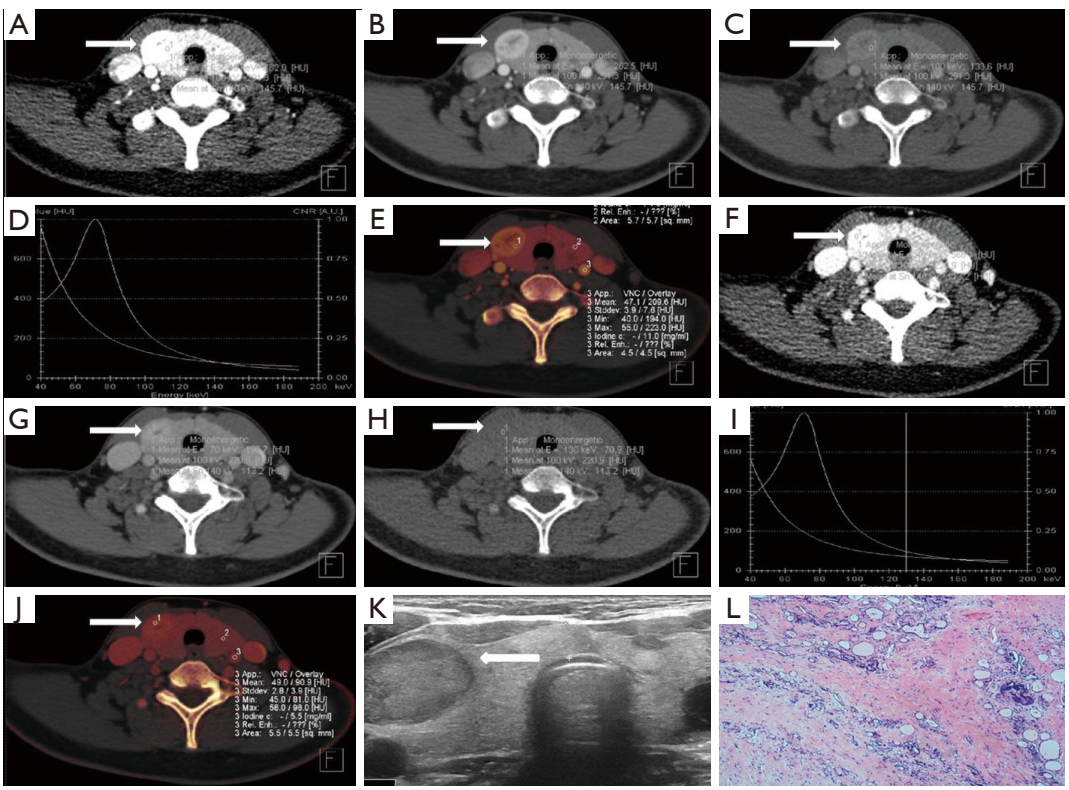

Figure 5 Images of benign thyroid nodules with DECT, US, and pathology. Images from a 48-year-old female patient with nodular goiter in the right lobe. (A-E) VMIs of 40, 70, and 100 keV, λ_{HU} and iodine map at arterial scan phase; (F-J) VMIs of 40, 70, 100keV, λ_{HU}, and iodine map at the venous scan phase; (K) grey scale image of US (TIRADS 4a); and (L) pathological image by hematoxylin-eosin staining (50×). White arrows pointed to thyroid nodule. DECT, dual-energy computed tomography; US, ultrasound; VMIs, virtual monochromatic images; λ_{HU}, slope of the spectral Hounsfield unit curve; TIRADS, Thyroid Imaging Report and Data System.

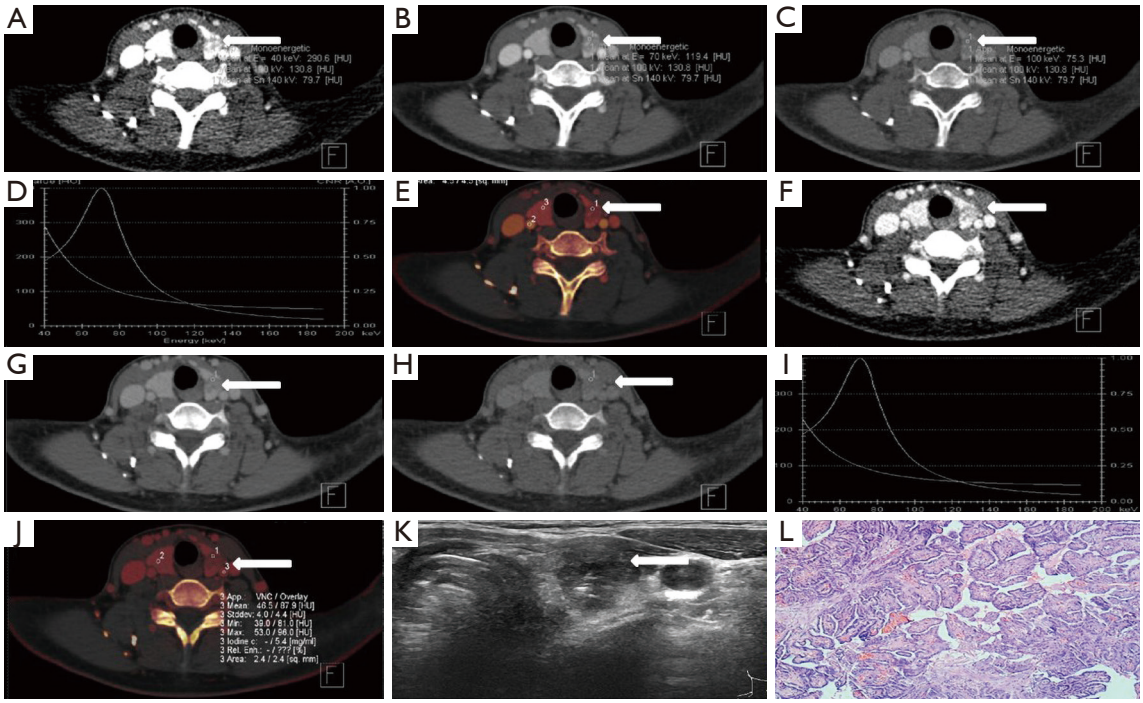

Figure 6 Images of malignant thyroid nodule with DECT, US, and pathology. Images from a 35-year-old female patient with papillary carcinoma in the left lobe. (A-E) VMIs of 40, 70, 100 keV, λ_{HU}, iodine map at arterial scan phase; (F-J) VMIs of 40, 70, 100keV, λ_{HU}, and iodine map at the venous scan phase; (K) grey scale image of US (TIRADS 4c); (L) pathological image by hematoxylin-eosin staining (50×). White arrows pointed to thyroid nodule. DECT, dual-energy computed tomography; US, ultrasound; VMIs, virtual monochromatic images; λ_{HU}, slope of the spectral Hounsfield unit curve; TIRADS, Thyroid Imaging Report and Data System.

DECT has been used to evaluate the response in patients with stage IV melanoma (38) after immunotherapy response, predict recurrence after radiotherapy (39), and improve the assessment of distant metastasis (40) beyond the differential diagnosis of thyroid nodules.

This study had a few limitations that should be noted. Firstly, some cases that did not include the histopathological assessment may have influenced the final results, because cytopathology from FNAB is not the gold standard. Secondly, cases enrolled in this study were not from multiple centers, which could have possibly influenced the statistical results. Thirdly, nodules with a background of nodular goiter in our study were relatively small, which may have influenced the precision of the DECT parameters.

In conclusion, DECT is useful for differentiating malignant from benign thyroid nodules, which has potential value in the indirect prediction of lymph node metastasis in thyroid carcinoma. Further research is required into the DECT multiparameters, and more data from multiple centers should be used to identify the application of DECT in thyroid nodules.

Acknowledgments

Funding: This study was funded by the Guangxi Scientific Research and Technology Development Plan (No. 1598011-4).

Footnote

Reporting Checklist: The authors have completed the STARD reporting checklist. Available at https://gs.amegroups.com/article/view/10.21037/gs-22-262/rc

Data Sharing Statement: Available at https://gs.amegroups.com/article/view/10.21037/gs-22-262/dss

Conflicts of Interest: All authors have completed the ICMJE uniform disclosure form (available at https://gs.amegroups.com/article/view/10.21037/gs-22-262/coif). All authors report that this study was funded by the Guangxi Scientific Research and Technology Development Plan (No. 1598011-4). The authors have no other conflicts of interest to declare.

Ethical Statement: The authors are accountable for all aspects of the work in ensuring that questions related to the accuracy or integrity of any part of the work are appropriately investigated and resolved. The study was conducted in accordance with the Declaration of Helsinki (as revised in 2013). The study was approved by the Medical Ethics Committee of First Affiliated Hospital of Guangxi Medical University [No. 2021(KY-E-034)]. Informed consent was taken from all the patients.

References

1. Vander JB, Gaston EA, Dawber TR. The significance of nontoxic thyroid nodules. Final report of a 15-year study of the incidence of thyroid malignancy. Ann Intern Med 1968;69:537-40.
2. Tunbridge WM, Evered DC, Hall R, et al. The spectrum of thyroid disease in a community: the Whickham survey. Clin Endocrinol (Oxf) 1977;7:481-93.
3. Tan GH, Gharib H. Thyroid incidentalomas: management approaches to nonpalpable nodules discovered incidentally on thyroid imaging. Ann Intern Med 1997;126:226-31.
4. Guth S, Theune U, Aberle J, et al. Very high prevalence of thyroid nodules detected by high frequency (13 MHz) ultrasound examination. Eur J Clin Invest 2009;39:699-706.
5. Shan Z, Chen L, Lian X, et al. Iodine Status and Prevalence of Thyroid Disorders After Introduction of Mandatory Universal Salt Iodization for 16 Years in China: A Cross-Sectional Study in 10 Cities. Thyroid 2016;26:1125-30.
6. Hegedüs L. Clinical practice. The thyroid nodule. N Engl J Med 2004;351:1764-71.
7. Mandel SJ. A 64-year-old woman with a thyroid nodule. JAMA 2004;292:2632-42.
8. Haugen BR, Alexander EK, Bible KC, et al. 2015 American Thyroid Association Management Guidelines for Adult Patients with Thyroid Nodules and Differentiated Thyroid Cancer: The American Thyroid Association Guidelines Task Force on Thyroid Nodules and Differentiated Thyroid Cancer. Thyroid 2016;26:1-133.
9. Gharib H, Papini E, Garber JR, et al. American Association of Clinical Endocrinologists, American College of Endocrinology, and Associazione Medici Endocrinologi Medical guidelines for clinical practice for the diagnosis and management of thyroid nodules--2016 update. Endocr Pract 2016;22:622-39.
10. Crippa S, Mazzucchelli L, Cibas ES, et al. The Bethesda System for reporting thyroid fine-needle aspiration specimens. Am J Clin Pathol 2010;134:343-4; author reply 345.
11. Forghani R. Advanced dual-energy CT for head and neck cancer imaging. Expert Rev Anticancer Ther 2015;15:1489-501.
12. Tawfik AM, Razek AA, Kerl JM, et al. Comparison of dual-energy CT-derived iodine content and iodine overlay of normal, inflammatory and metastatic squamous cell carcinoma cervical lymph nodes. Eur Radiol 2014;24:574-80.
13. Li M, Zheng X, Li J, et al. Dual-energy computed tomography imaging of thyroid nodule specimens: comparison with pathologic findings. Invest Radiol 2012;47:58-64.
14. Grant EG, Tessler FN, Hoang JK, et al. Thyroid Ultrasound Reporting Lexicon: White Paper of the ACR Thyroid Imaging, Reporting and Data System (TIRADS) Committee. J Am Coll Radiol 2015;12:1272-9.
15. Tessler FN, Middleton WD, Grant EG, et al. ACR Thyroid Imaging, Reporting and Data System (TI-RADS): White Paper of the ACR TI-RADS Committee. J Am Coll Radiol 2017;14:587-95.
16. Kwak JY, Han KH, Yoon JH, et al. Thyroid imaging reporting and data system for US features of nodules: a step in establishing better stratification of cancer risk. Radiology 2011;260:892-9.
17. Yoshizumi T. Dual Energy CT in Clinical Practice. Med Phys 2011;38:6346.
18. Bray F, Ferlay J, Soerjomataram I, et al. Global cancer statistics 2018: GLOBOCAN estimates of incidence and mortality worldwide for 36 cancers in 185 countries. CA Cancer J Clin 2018;68:394-424.
19. Zhang Y, Zhou P, Tian SM, et al. Usefulness of combined use of contrast-enhanced ultrasound and TI-RADS classification for the differentiation of benign from malignant lesions of thyroid nodules. Eur Radiol 2017;27:1527-36.
20. Cantisani V, D'Andrea V, Biancari F, et al. Prospective evaluation of multiparametric ultrasound and quantitative elastosonography in the differential diagnosis of benign

and malignant thyroid nodules: preliminary experience. Eur J Radiol 2012;81:2678-83.
21. Solbiati L, Osti V, Cova L, et al. Ultrasound of thyroid, parathyroid glands and neck lymph nodes. Eur Radiol 2001;11:2411-24.
22. Dohán O, Baloch Z, Bánrévi Z, et al. Rapid communication: predominant intracellular overexpression of the Na(+)/I(-) symporter (NIS) in a large sampling of thyroid cancer cases. J Clin Endocrinol Metab 2001;86:2697-700.
23. Portulano C, Paroder-Belenitsky M, Carrasco N. The Na+/I- symporter (NIS): mechanism and medical impact. Endocr Rev 2014;35:106-49.
24. Riesco-Eizaguirre G, Rodríguez I, De la Vieja A, et al. The BRAFV600E oncogene induces transforming growth factor beta secretion leading to sodium iodide symporter repression and increased malignancy in thyroid cancer. Cancer Res 2009;69:8317-25.
25. Galrão AL, Camargo RY, Friguglietti CU, et al. Hypermethylation of a New Distal Sodium/Iodide Symporter (NIS) enhancer (NDE) is associated with reduced NIS expression in thyroid tumors. J Clin Endocrinol Metab 2014;99:E944-52.
26. Jiang L, Liu D, Long L, et al. Dual-source dual-energy computed tomography-derived quantitative parameters combined with machine learning for the differential diagnosis of benign and malignant thyroid nodules. Quant Imaging Med Surg 2022;12:967-78.
27. Liou MJ, Lin JD, Chan EC, et al. Detection of mRNA of sodium iodide symporter in benign and malignant human thyroid tissues. Cancer Lett 2000;160:75-80.
28. Smanik PA, Ryu KY, Theil KS, et al. Expression, exon-intron organization, and chromosome mapping of the human sodium iodide symporter. Endocrinology 1997;138:3555-8.
29. Matsumoto K, Jinzaki M, Tanami Y, et al. Virtual monochromatic spectral imaging with fast kilovoltage switching: improved image quality as compared with that obtained with conventional 120-kVp CT. Radiology 2011;259:257-62.
30. Pinho DF, Kulkarni NM, Krishnaraj A, et al. Initial experience with single-source dual-energy CT abdominal angiography and comparison with single-energy CT angiography: image quality, enhancement, diagnosis and radiation dose. Eur Radiol 2013;23:351-9.
31. Patel BN, Thomas JV, Lockhart ME, et al. Single-source dual-energy spectral multidetector CT of pancreatic adenocarcinoma: optimization of energy level viewing significantly increases lesion contrast. Clin Radiol 2013;68:148-54.
32. Li M, Zheng X, Gao F, et al. Spectral CT imaging of intranodular hemorrhage in cases with challenging benign thyroid nodules. Radiol Med 2016;121:279-90.
33. Yang L, Luo D, Li L, et al. Differentiation of malignant cervical lymphadenopathy by dual-energy CT: a preliminary analysis. Sci Rep 2016;6:31020.
34. Zou Y, Zhang H, Li W, et al. Prediction of ipsilateral lateral cervical lymph node metastasis in papillary thyroid carcinoma: a combined dual-energy CT and thyroid function indicators study. BMC Cancer 2021;21:221.
35. Qiu L, Hu J, Weng Z, et al. A prospective study of dual-energy computed tomography for differentiating metastatic and non-metastatic lymph nodes of colorectal cancer. Quant Imaging Med Surg 2021;11:3448-59.
36. Liu X, Ouyang D, Li H, et al. Papillary thyroid cancer: dual-energy spectral CT quantitative parameters for preoperative diagnosis of metastasis to the cervical lymph nodes. Radiology 2015;275:167-76.
37. Zhao Y, Li X, Li L, et al. Preliminary study on the diagnostic value of single-source dual-energy CT in diagnosing cervical lymph node metastasis of thyroid carcinoma. J Thorac Dis 2017;9:4758-66.
38. Brendlin AS, Peisen F, Almansour H, et al. A Machine learning model trained on dual-energy CT radiomics significantly improves immunotherapy response prediction for patients with stage IV melanoma. J Immunother Cancer 2021;9:e003261.
39. Bahig H, Lapointe A, Bedwani S, et al. Dual-energy computed tomography for prediction of loco-regional recurrence after radiotherapy in larynx and hypopharynx squamous cell carcinoma. Eur J Radiol 2019;110:1-6.
40. Lenga L, Czwikla R, Wichmann JL, et al. Dual-energy CT in patients with colorectal cancer: Improved assessment of hypoattenuating liver metastases using noise-optimized virtual monoenergetic imaging. Eur J Radiol 2018;106:184-91.

(English Language Editor: A. Kassem)

Cite this article as: Li F, Huang F, Liu C, Pan D, Tang X, Wen Y, Chen Z, Qin Y, Chen J. Parameters of dual-energy CT for the differential diagnosis of thyroid nodules and the indirect prediction of lymph node metastasis in thyroid carcinoma: a retrospective diagnostic study. Gland Surg 2022;11(5):913-926. doi: 10.21037/gs-22-262